



OPEN

Comparison between bone–implant interfaces of microtopographically modified zirconia and titanium implants

Myint Kyaw Thu^{1,4}, Young Suk Kang^{2,4}, Jeong Min Kwak^{1,4}, Ye-Hyeon Jo³, Jung-Suk Han¹ & In-Sung Luke Yeo¹✉

The aim of this study was to investigate the surface characteristics and evaluate the bone–implant interfaces of injection molded zirconia implants with or without surface treatment and compare them with those of conventional titanium implants. Four different zirconia and titanium implant groups ($n = 14$ for each group) were prepared: injection-molded zirconia implants without surface treatment (IM ZrO₂); injection-molded zirconia implants with surface treatment via sandblasting (IM ZrO₂-S); turned titanium implants (Ti-turned); and titanium implants with surface treatments via sandblasting with large-grit particles and acid-etching (Ti-SLA). Scanning electron microscopy, confocal laser scanning microscopy, and energy dispersive spectroscopy were used to assess the surface characteristics of the implant specimens. Eight rabbits were used, and four implants from each group were placed into the tibiae of each rabbit. Bone-to-implant contact (BIC) and bone area (BA) were measured to evaluate the bone response after 10-day and 28-day healing periods. One-way analysis of variance with Tukey's pairwise comparison was used to find any significant differences. The significance level was set at $\alpha = 0.05$. Surface physical analysis showed that Ti-SLA had the highest surface roughness, followed by IM ZrO₂-S, IM ZrO₂, and Ti-turned. There were no statistically significant differences ($p > 0.05$) in BIC and BA among the different groups according to the histomorphometric analysis. This study suggests that injection-molded zirconia implants are reliable and predictable alternatives to titanium implants for future clinical applications.

Abbreviations

Ti	Titanium
ZrO ₂	Zirconia; zirconium dioxide
SLA	Sandblasted with large-grit particles and acid-etched
IM ZrO ₂	Injection-molded zirconia implant
IM ZrO ₂ -S	Injection-molded zirconia implant with sandblasting surface treatment
Ti-turned	Turned titanium implant
Ti-SLA	Titanium implant with SLA surface treatment
BIC	Bone-to-implant contact
BA	Bone area
CNC	Computer numerical control
FE-SEM	Field emission-scanning electron microscopy
CLSM	Confocal laser scanning microscopy
EDS	Energy dispersive spectroscopy
ARRIVE	Animal research: reporting in vivo experiments
XRD	X-ray diffraction

¹Department of Prosthodontics, School of Dentistry and Dental Research Institute, Seoul National University, 101, Daehak-ro, Jongro-gu, Seoul 03080, Korea. ²618th Medical Company (Dental Area Support)/Dental Health Activity-Korea, Camp Humphreys, APO, AP 96297, USA. ³Dental Research Institute, Seoul National University, Seoul 03080, Korea. ⁴These authors contributed equally: Myint Kyaw Thu, Young Suk Kang and Jeong Min Kwak. ✉email: pros53@snu.ac.kr

m-ZrO ₂	Monoclinic zirconia
t-ZrO ₂	Tetragonal zirconia

Implant dentistry has become a predictable and reliable treatment modality for restoring the esthetics and functions of partially and completely edentulous patients. For successful outcomes of implant-supported dental prostheses, osseointegration, the biological fixation of an implant defined as direct bone-to-implant contact (BIC) without an intervening connective tissue layer, must be achieved^{1,2}. Therefore, BIC is a critical indicator for successful osseointegration, which governs the long-term clinical success and survival of implant-supported dental prostheses³. For the optimal BIC, the surface characteristics, both physical and chemical, of dental implants play a critical role in the osseointegration process.

Over the last 40 years, both commercially pure titanium (Ti) and titanium alloys have been used for dental implants due to their excellent biocompatibility, mechanical strength, chemical inertness, and high clinical success rates⁴. Since the 1990s, various microtopographical modification methods for Ti implant surfaces have been introduced by implant manufacturers to accelerate early osseous integration and increase the resistance of the bone–implant interface to functional loading⁵. Among them, roughening Ti implant surfaces at the microscopic level with sandblasting and acid-etching has become very popular due to its high success rate⁶. However, the main disadvantage of Ti implants is their dark grayish color, which may lead to esthetic compromise if buccal bone loss and unfavorable soft-tissue response in gingival biotypes occur⁷.

Therefore, researchers have developed zirconia (zirconium dioxide, ZrO₂) implants in the last 2 decades to mitigate the esthetic disadvantage of titanium implants^{8,9}. The main advantage of ZrO₂ implants is their tooth-like color, which makes them superior to Ti implants in esthetically critical locations, such as the maxillary anterior area. In addition, they possess promising characteristics, such as a high resistance to wear and corrosion, high fracture resistance and flexural strength, biocompatibility, minimal ion-release, and reduced bacterial adhesion and plaque accumulation^{10–12}. However, ZrO₂ also has disadvantages, such as a sensitivity to low-temperature degradation (aging), vulnerability to subcritical bending and crack growth, and lower fracture resistance, compared to titanium^{13,14}. It is also challenging to roughen ZrO₂ implant surfaces because of their hardness¹⁵. In the literature, various attempts to modify ZrO₂ surfaces have been reported, such as sandblasting, etching with hydrochloric or hydrofluoric acids¹⁶, the aggregation of bioactive materials such as hydroxyapatite¹⁷, plasma spraying¹⁸, ultraviolet radiation to induce the hydrophilicity of ZrO₂¹⁹, and selective infiltration-etching techniques to create a nanoporous surface²⁰.

Although both the additive manufacturing and subtractive (milling) manufacturing of ZrO₂ by computer-aided design and computer-aided manufacturing (CAD/CAM) technology have been studied frequently, as reported in the literature^{21–23}, the injection molding of ZrO₂ has been reported in the literature since the 1980s²⁴. This technique is a type of plasticity-shaping technique that utilizes a binder, plasticizer, lubricant, and coupling agent²⁵. The process begins with compounding fine ceramic powders with a blend of polymers or wax in solvent. Then, the organic binders embedded in the molds are removed via thermal pyrolysis or solvent detracting before sintering²⁶. Injection molding is suitable for making relatively fine ceramic parts because it offers dimensional reproducibility, requires little or no modification, and produces parts with a sufficient quality for clinical applications²⁷. In particular, this technique allows the mass production of ceramic parts at low cost and near-net-shape formation²⁸.

Previous animal studies and various case reports have indicated that the osseointegration of ZrO₂ implants is similar to or even superior to that of Ti implants^{29–31}. However, the effects of different surface characteristics (i.e., smooth vs. rough) of ZrO₂ implants on the osseointegration process are still largely unknown³². Furthermore, there is no report on the early bone response around injection-molded ZrO₂ implants compared to that around Ti implants. This *in vivo* study aimed to compare the bone–implant interfaces of injection-molded ZrO₂ implants and computer numerical control (CNC)-machined Ti implants. Two types of surfaces were prepared for each material: sandblasted and nonsandblasted surfaces for the injection-molded ZrO₂ implants and sandblasted, large-grit, acid-etched (SLA) and non-SLA surfaces for the CNC-machined Ti implants. The surface characteristics of the implants were also investigated. The hypothesis underlying this study was that the hard-tissue response to the injection-molded ZrO₂ implants is similar to the osseointegration of Ti implants with SLA surfaces, which are used in dental clinics worldwide.

Methods

Preparation of implant samples. A total of 56 screw-shaped dental implant samples (28 ZrO₂ implants (one-piece) and 28 Ti implants) of the same macroscopic shape and dimensions (a diameter of 3.4 mm and a length of 8 mm) were used in this study. Also, ten ZrO₂ discs, which were 15 mm in diameter and 1 mm in thickness, were prepared to find some phase transition of ZrO₂ after surface modification. The ZrO₂ implants were manufactured using an injection molding technique (Vatech Acucera, Seoul, Korea). This process involves mixing zirconia powders with modifiers and shaping a uniform and homogeneous mixture into a mold. The Ti implants were manufactured by a computer numerical controlled (CNC) milling technique (Deep Implant System, Inc., Seongnam, Korea). Disc-shaped green compacts were prepared by cold isostatic press of powder mixtures and then sintered. Surface modification with sandblasting was performed on half of the ZrO₂ implants and the ZrO₂ discs, while half of the Ti implant samples were surface-modified with SLA treatment, i.e., sandblasted with large-grit alumina (Al₂O₃) particles and etched with hydrochloric acid (SLA surface; Deep Implant System, Inc., Seongnam, Korea). After sandblasting, the ZrO₂ implants (14 implants) and discs (5 discs) were treated by hot isostatic pressing (HIP) at 1380 °C and 138 MPa. Then, the samples were divided into four experimental groups:

- (1) Group 1 = IM ZrO₂ (injection-molded ZrO₂ implants or ZrO₂ discs without sandblasting modification)
- (2) Group 2 = IM ZrO₂-S (injection-molded ZrO₂ implants or ZrO₂ discs with sandblasting modification)
- (3) Group 3 = Ti-turned (Ti implants without SLA modification as a negative control)
- (4) Group 4 = Ti-SLA (Ti implants with SLA modification as a positive control)

Assessment of surface characteristics. The implant sample surfaces were photographed by field emission-scanning electron microscopy (FE-SEM; S-4700, Hitachi, Tokyo, Japan). Surface parameters for the sample topography were measured by confocal laser scanning microscopy (CLSM; LSM 800, Carl Zeiss AG, Oberkochen, Germany). The acquired images were analyzed using ConfoMap software, and specific areas of interest were selected. Subsequently, the surface topography was quantified in terms of Sa (arithmetical mean height of a surface), the absolute value of the difference in height of each point compared to the arithmetical mean of the surface, and Sdr (developed interfacial area ratio), the proportion of the additional surface area contributed by the texture within the defined planar area. Each sample was analyzed at 3 selected sites (the upper, middle and lower flank), the values of which were averaged, and the average value was assigned as the representative value for the sample^{22,33}. The topography was measured in terms of Sa values (arithmetical mean height) and Sdr values (developed interfacial area ratio). In addition, the chemical composition of each sample was analyzed with an energy-dispersive spectroscopy (EDS) device (EMAX, Horiba, High Wycombe, United Kingdom). For evaluating the phase transition of ZrO₂, the ZrO₂ disc surfaces were analyzed using a high resolution X-ray diffractometer (SmartLab, Rigaku, Tokyo, Japan) with Cu K α radiation (wavelength = 1.54 Å) and 45 kV/200 mA. To quantify the molar fraction of the content of monoclinic ZrO₂ (X_m), the following equations were employed:

$$X_m = \frac{I_m(111) + I_m(\bar{1}\bar{1}\bar{1})}{I_m(111) + I_m(\bar{1}\bar{1}\bar{1}) + I_t(101)}$$

where I_t and I_m represent the intensity of the tetragonal (101) and monoclinic (111) and ($\bar{1}\bar{1}\bar{1}$) peaks^{34,35}. The peak intensity was obtained using MDI Jade 6 software (Materials Data Inc., Livermore, CA, USA).

In vivo surgery. Eight male New Zealand white rabbits (age: 3–4 months old; weight: 2.5–3.0 kg) were used in this in vivo study, which was approved by the Institutional Animal Research Ethics Committee of Cronex (CRONEX-IACUC: 202108011, Hwaseong, Korea) and conducted according to the Animal Research: Reporting In Vivo Experiments (ARRIVE) guidelines³⁶. All methods were performed in accordance with the relevant guidelines and regulations. The experimental animals acclimatized in separate cages for two weeks before surgery. Each rabbit received four implant samples; two implants were placed in each tibia bone of the hind legs. The ZrO₂ and Ti implants were inserted based on the split-plot design (Fig. 1). For anesthesia, a combination of 15 mg/kg tiletamine hydrochloride and zolazepam hydrochloride (Zoletil 50; Virbac Korea Co., Ltd., Seoul, Korea) and 5 mg/kg xylazine (Rompun; Bayer Korea, Ltd., Seoul, Korea) was administered intramuscularly. Then, the hind legs were shaved and disinfected with an antiseptic surgical scrub of 7.5% povidone-iodine (Beta-dine; Korea Pharma, Seoul, Korea). After site preparation, local infiltration anesthesia of 2% lidocaine hydrochloride with 1:100,000 epinephrine (Yuhan Company, Seoul, Korea) was administered at the surgical sites. The tibial bones were exposed by full-thickness incisions from the skin to the periosteum. The surgical sites on the tibiae bones were prepared with rotating implant drills and engines under copious irrigation with sterile saline solution. The final drill size was 3.0 mm, and 32 sample implants from experimental groups 1, 2, 3 and 4 were placed with primary stability (≥ 20 Ncm) using a torque wrench, according to the manufacturer's instructions. After the implant placement surgeries, the muscle and fascia were sutured with resorbable 4–0 Vicryl sutures (Coated Vicryl; Ethicon, Raritan, NJ, United States), and the outer dermis was closed with nylon (Blue nylon; Ailee, Busan, Korea). All rabbit specimens were housed in individual cages and administered the postoperative antibiotic prophylaxis of enrofloxacin (Biotril, Komipharm International, Siheung, Korea).

Assessment of histology and histomorphometry. Four rabbits were sacrificed 10 days after the implant placement (Rabbit 1–4), and the remaining 4 rabbits were sacrificed 28 days after the implant placement (Rabbit 5–8) by an overdose of potassium chloride intravenously under anesthesia for histologic assessment. The bones and connective tissues that surrounded the implant samples were surgically harvested en bloc. These blocks were fixed in 10% neutral buffered formalin for two weeks and then dehydrated with ethanol, followed by embedding in light-curing resin (Technovit 7200 VLC, Kulzer, Wehrheim, Germany). A series of cutting and grinding devices (EXAKT system; EXAKT Apparatebau, Norderstedt, Germany) was used to cut and grind the embedded blocks into slides with a thickness of less than approximately 50 μm ^{22,37}. The slides were stained with modified Goldner's Masson trichrome staining solution for examination under a light microscope. This staining technique allows for easy discrimination between newly formed bone (stained red) and existing mature bone (stained blue)³⁸. The bone-to-implant interfaces were measured by the degree of BIC and bone area (BA) at the best three consecutive threads^{22,39}. The histologic evaluation was performed using a light microscope (DM2700M, Leica Microsystems CMS GmbH, Wetzlar, Germany) and an attached digital camera (DMC5400, Leica Microsystems CMS GmbH, Wetzlar, Germany). An image analysis system (ImageJ 1.60, NIH, Bethesda, MD, United States) was used to analyze the acquired images.

Statistical analysis. Most of the outcome variables for data normalization were accepted when the Shapiro–Wilk test was used ($p > 0.05$). Descriptive statistics are shown as the means and standard deviations (SDs). One-way analysis of variance (ANOVA) was used to analyze differences in the mean values of the surface param-

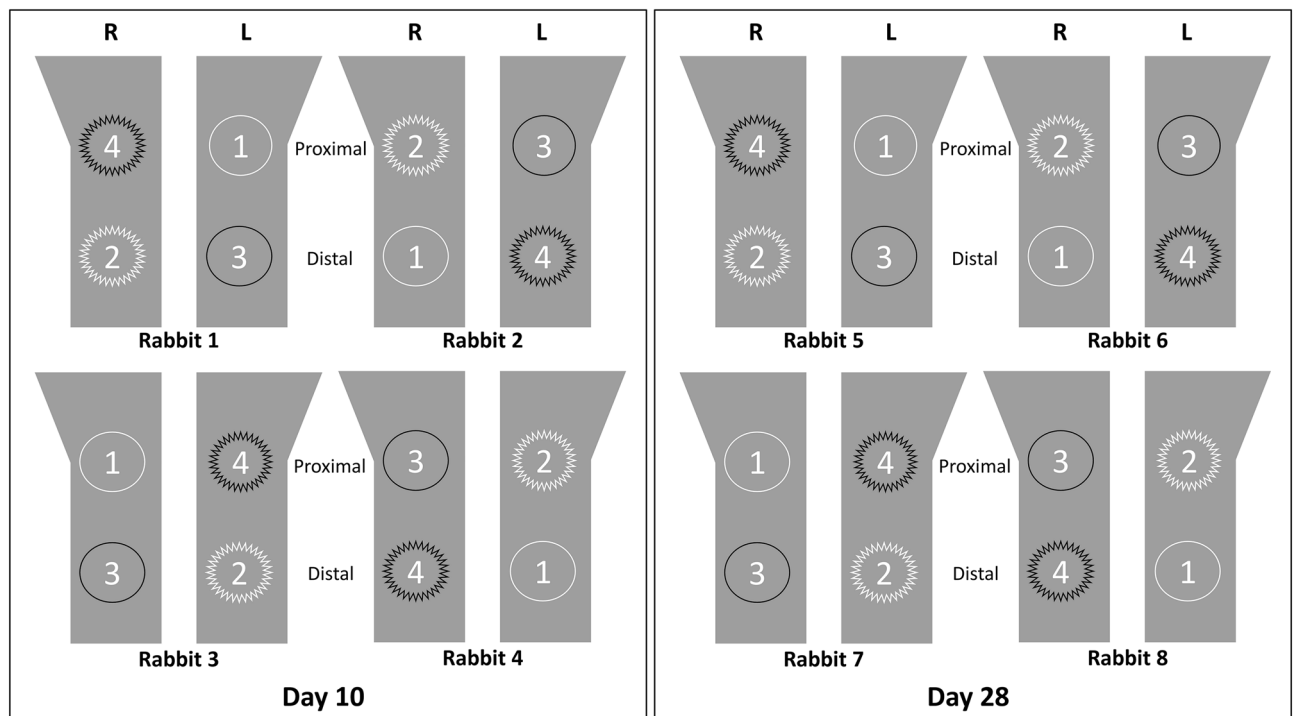


Figure 1. Four implant groups used in this study. 1: injection-molded ZrO₂ implant; 2: sandblasted injection-molded ZrO₂ implant; 3: turned Ti implant; 4: SLA Ti implant. This schematic diagram shows that these implants were placed in rabbit tibiae according to the split-plot design. The saw-edged circles represent the implants whose surfaces were microtopographically modified, while the smooth edged ones represent implants with no microtopographical modification. Black represents Ti, and white represents ZrO₂. R = right tibia; L = left tibia.

eters and histomorphometric data of the different types of implants in this study. When a significant difference was found, Tukey's honestly significant difference (HSD) was further applied for a pairwise comparison. In addition, the independent t test was used to compare the BIC and BA values of the 2 healing periods (10 days vs. 28 days). Statistical software, R version 4.1.0 (R Foundation for Statistical Computing, Vienna, Austria), was used for all statistical evaluations. The statistical significance level was set at $\alpha = 0.05$.

Ethics approval and consent to participate. Ethical approval was sought from the Institutional Animal Care and Use Committee of CRONEX Co., Ltd., Hwaseong, Korea, and the animal experiment was conducted in accordance with the Animal Reporting in Vivo Experiments (ARRIVE) guidelines (202108011).

Consent for publication. All authors are aware of the publication of this work.

Results

Surface characteristics. The FE-SEM images of the implant surfaces of the 4 different experimental groups are shown in Fig. 2A. The IM ZrO₂ (Group 1) implants showed microcracks, porosities, and grain structures that are typically observed for sintered ZrO₂. In contrast, the IM ZrO₂-S (Group 2) implants showed very rough surfaces with slate-like profiles and lower porosities. The Ti-turned (Group 3: negative control) implants showed smooth and flat surfaces with continuous straight lines that ran in one direction. However, the Ti-SLA (Group 4: positive control) implants exhibited a rough, irregular, porous, and honeycomb-like appearance.

The surface roughness parameters of the experimental groups were measured in terms of Sa and Sdr values (Fig. 2B,C). Based on the mean Sa values and SDs, the Ti-SLA implants had the highest Sa value ($1.68 \mu\text{m} \pm 0.07 \mu\text{m}$), followed by the IM ZrO₂-S implants ($1.10 \mu\text{m} \pm 0.13 \mu\text{m}$), IM ZrO₂ implants ($0.64 \mu\text{m} \pm 0.12 \mu\text{m}$), and Ti-turned implants ($0.52 \mu\text{m} \pm 0.21 \mu\text{m}$). There were statistically significant differences among the Sa values of all groups, except between the IM ZrO₂ and Ti-turned groups. The mean Sdr values of the Ti-SLA implants ($238.78\% \pm 3.03\%$) were significantly higher than those of the other three groups. However, there were no significant differences among the Sdr values of these three groups: IM ZrO₂ ($49.04\% \pm 31.68\%$), IM ZrO₂-S ($78.77\% \pm 50.02\%$), and Ti-turned ($123.66\% \pm 37.54\%$).

The EDS findings are shown in Table 1. Titanium (Ti), carbon (C), and oxygen (O) were detected in the Ti implants, while zirconium (Zr), carbon (C), and oxygen (O) were detected in the ZrO₂ implants. The X-ray diffraction patterns of the ZrO₂ discs are shown in Fig. 3. ZrO₂ discs without sandblasting modification only presented the tetragonal ZrO₂ peak. ZrO₂ discs with sandblasting modification presented the (111) and ($\bar{1}\bar{1}\bar{1}$) peaks for the monoclinic phase (m-ZrO₂) and the (101) peak for the tetragonal phase (t-ZrO₂). However, it was

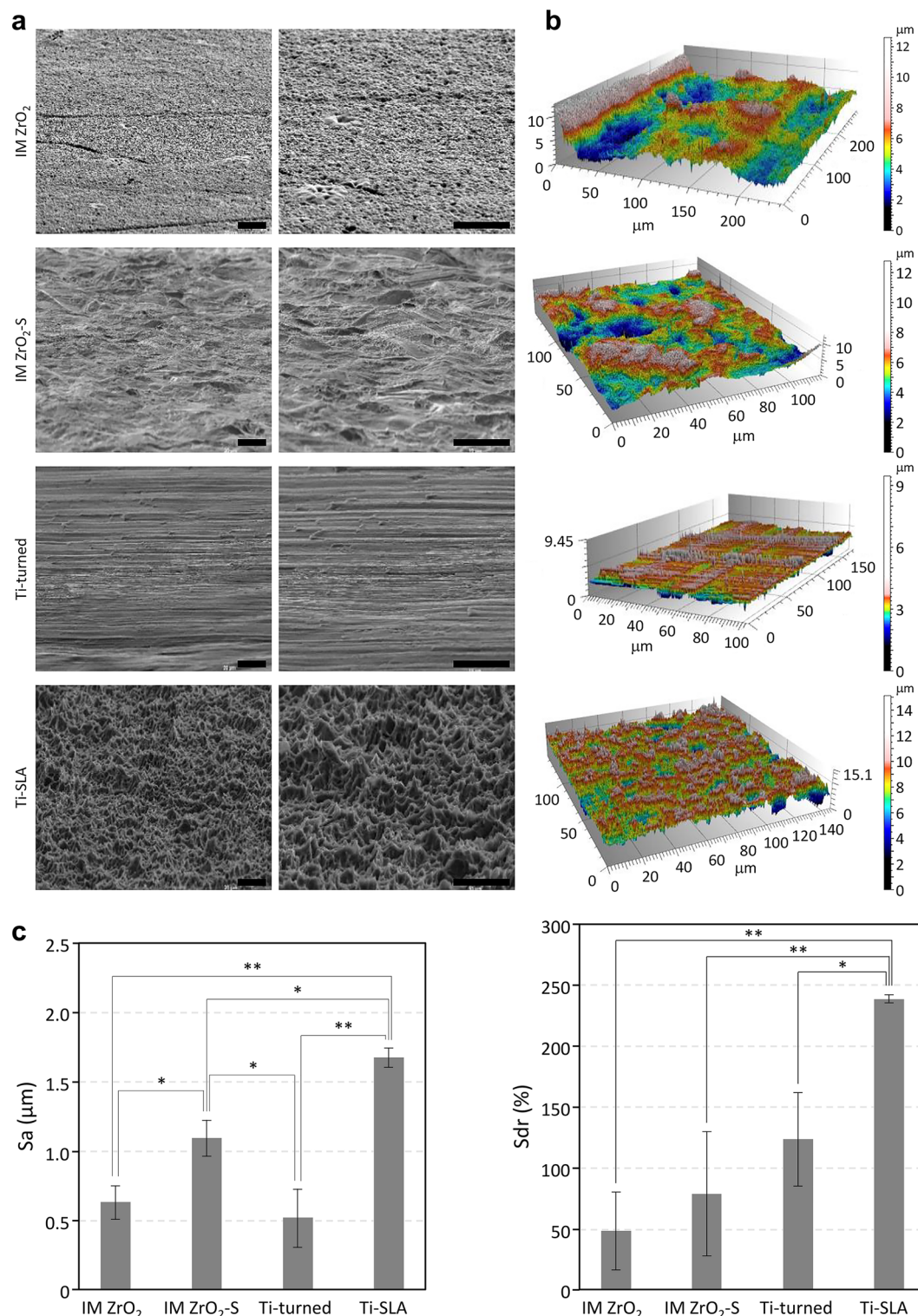


Figure 2. Surface characteristics of the ZrO₂ and Ti specimens investigated in this study. **(a)** FE-SEM images of the surfaces of IM ZrO₂ (injection-molded zirconia without surface treatment), IM ZrO₂-S (injection-molded zirconia implant with sandblasting surface treatment), Ti-turned (turned titanium implant), and Ti-SLA (SLA titanium implant) at 2000× (left) and 5000× (right) magnifications. Scale bars = 10 μm. **(b)** CLSM images of surface roughness of implant surfaces (3D views of color-coded height maps with texture overlay). **(c)** Surface roughness parameters (Sa and Sdr) of the implant surfaces. Data are presented as the means ± SDs (n = 3). **p* < 0.05 and ***p* < 0.01.

Group (n = 3)	Atomic percentage (%)				
	C	O	N	Zr	Ti
IM ZrO ₂	56.67	07.47	0.00	35.85	00.00
IM ZrO ₂ -S	48.58	24.56	0.00	26.85	00.00
Ti-turned	05.56	11.86	0.00	00.00	82.54
Ti-SLA	04.04	14.24	0.00	00.00	81.72

Table 1. Element composition analysis of the ZrO₂ and Ti implant surfaces according to energy dispersive spectroscopy. C carbon, O oxygen, N nitrogen, Zr zirconium, Ti titanium.

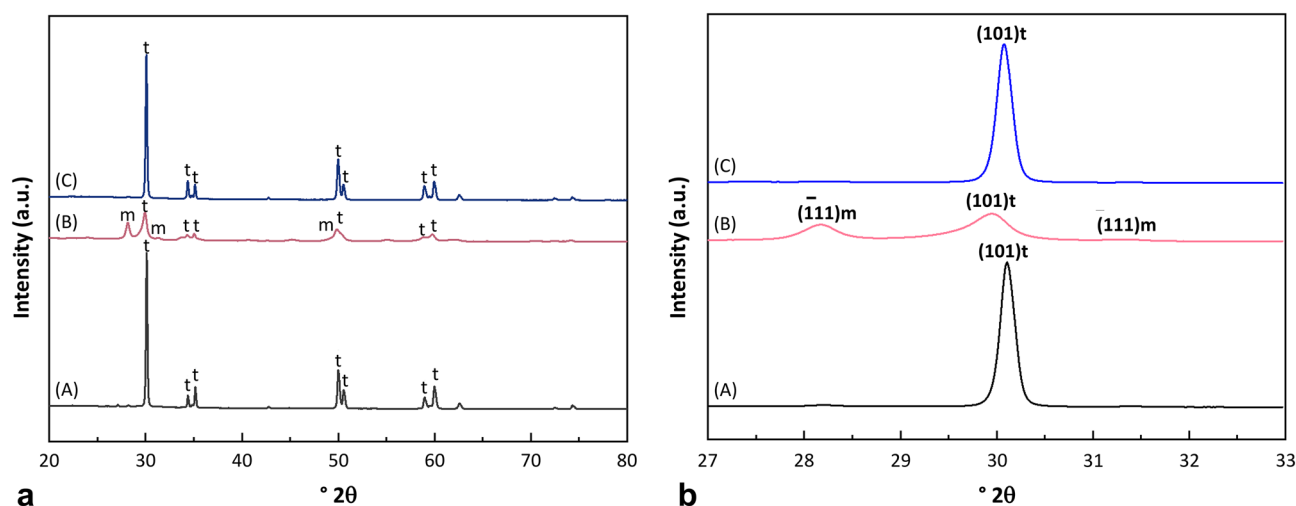


Figure 3. X-ray diffraction (XRD) patterns of the ZrO₂ discs (a) in the range of 20–80° 2θ are presented. More detailed XRD patterns are also shown in the range of 27–33° 2θ (b). Compared to the XRD peaks of the ZrO₂ discs before sandblasting (A), the presence of the monoclinic phase was detected after the ZrO₂ discs were sandblasted (B). The monoclinic phase disappeared upon hot isostatic pressing of the sandblasted ZrO₂ discs (C).

clearly seen that while the ZrO₂ discs with sandblasting modification presented both the peaks corresponding to the tetragonal and monoclinic phases, only the peak of tetragonal phase was detected after HIP. As seen in Table 2, the rate of the tetragonal-to-monoclinic phase transformation increased with sandblasting modification. It was found that the amount of m-ZrO₂ was 40.32% of the total ZrO₂ after sandblasting modification. After HIP, this amount of monoclinic phase was totally transformed into t-ZrO₂.

Analysis of histology and histomorphometry. All the implant samples successfully osseointegrated after 10 days of healing and 28 days of healing (Supplementary Fig. S1). In the histological analysis of the ZrO₂ and Ti implants stained with modified Goldner's Masson trichrome staining solution, new bone formation was found along the bone-implant interfaces. In the cortical bone area of the tibiae, the exiting mature bones were stained blue, while newly formed immature bones were stained red and detected at the implant threads and around the mature bone (Fig. 4).

The mean BIC and BA values and SDs of the ZrO₂ and Ti implants at the 10-day and 28-day marks are shown in Fig. 5 (Supplementary Tables S1, S2). Although the BICs (%) of the IM ZrO₂-S and Ti-SLA implants were higher than those of the Ti-turned and IM ZrO₂ implants at the 10-day mark, the differences were not statistically significant. At the 28-day mark, the BIC (%) of the Ti-SLA implants was significantly higher than that of the Ti-turned implants ($p = 0.04$). However, the other groups showed no significant differences. When the mean values and SDs of BA (%) were calculated, no statistically significant differences were found among the ZrO₂ and Ti implants for both healing periods ($p > 0.05$) (Fig. 5).

m-ZrO ₂ *	Without sandblasting	With sandblasting	After HIP [†]
Mean (SD)	1.03 (0.09)	40.32 (5.97)	0.50 (0.07)

Table 2. The tetragonal-to-monoclinic phase transformation in ZrO₂ discs with and without sandblasting modification and after HIP. *Monoclinic ZrO₂. [†]Hot isostatic pressing.

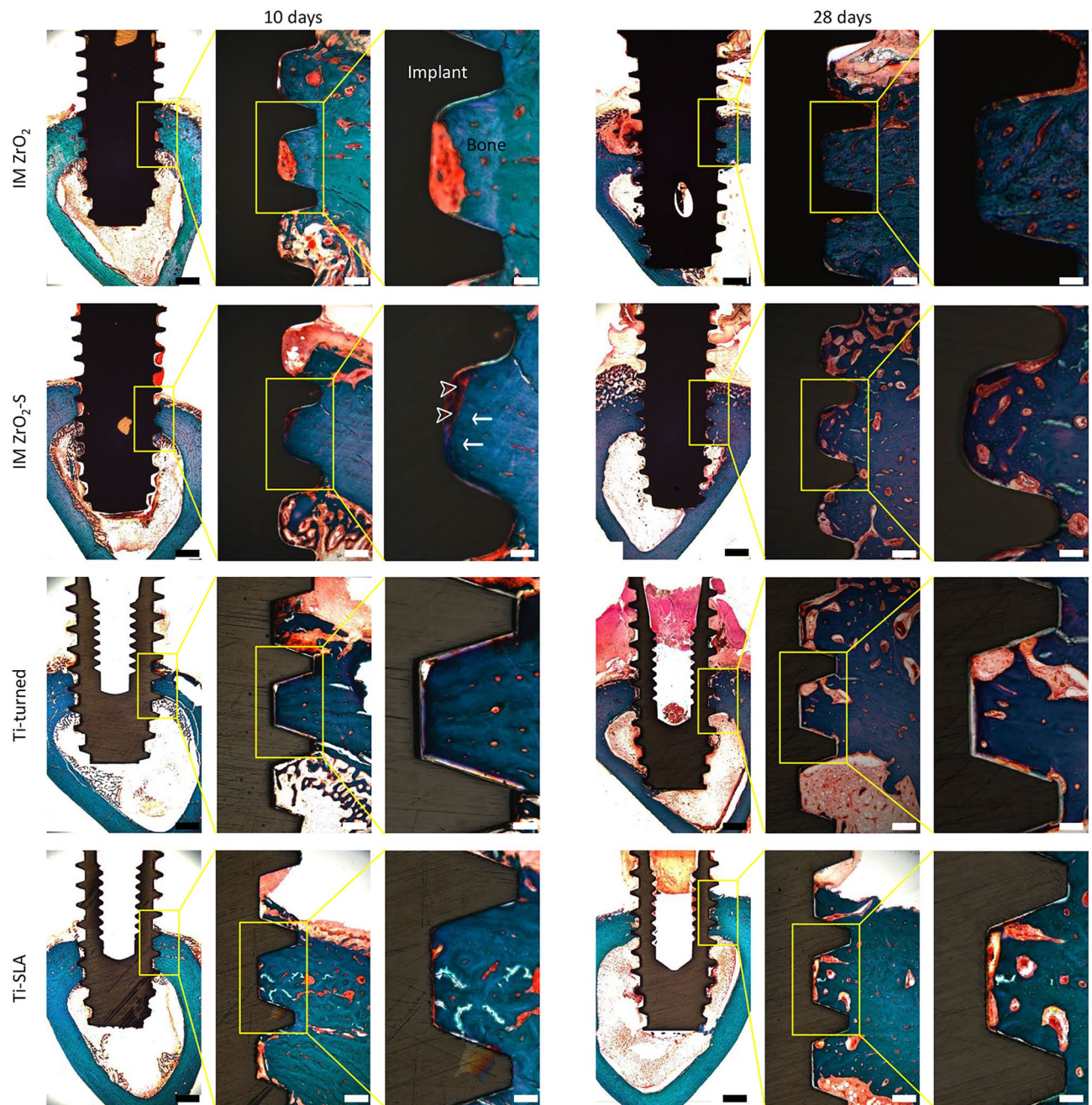


Figure 4. Histological views and histomorphometric data for bone responses to the ZrO₂ and Ti implants. Light microscopic views of the implants with modified Goldner's Masson trichrome staining at 10 and 28 days after installation into rabbit tibiae (scale bars from left to right: 1 mm at $\times 12.5$, 200 μm at $\times 50$, and 100 μm at $\times 100$ magnification). The exiting mature bone was stained blue (white arrow), and new immature bone or osteoid was stained red (white-edged arrowhead) at the bone–implant interfaces.

Discussion

The roughness parameters (Sa and Sdr) of the surface-treated implants (Groups 2 and 4) were significantly higher than those of the ZrO₂ and Ti implant groups without surface treatment (Groups 1 and 3). The authors also found that the BIC% and BA% of the IM ZrO₂ implants were not significantly different from those of the Ti implants (both Ti-turned and Ti-SLA) after 10-day and 28-day healing periods. These results are in agreement with the findings of previous studies that compared SLA-treated IM ZrO₂ and Ti implants in mini pig maxillae models⁴⁰, canine models⁴¹, and rabbit tibia models⁴². Another significant finding was that the surface-treated ZrO₂ implants showed enhanced bone integration at the implant surface compared to the untreated ZrO₂ implants. This finding is in line with the results of other studies by Mihatovic in 2017 and Schünemann in 2019^{43,44}. In addition, the Ti-SLA implants demonstrated a significantly higher bone response than the Ti-turned implants. This finding is also comparable to findings in other studies^{45,46}. It can be deduced that the rough surface microtopography of

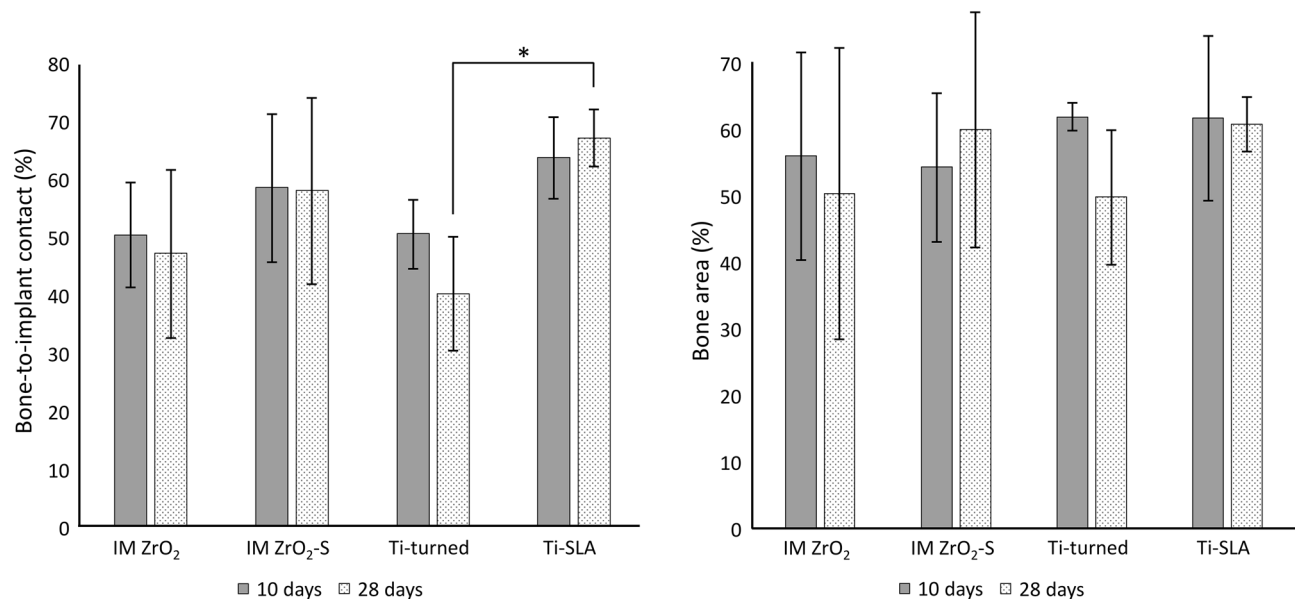


Figure 5. The mean and standard deviation of bone-to-implant contact (left) and bone area (right) ratios of the implants at 10 and 28 days after installation ($n = 4$). $*p < 0.05$.

ZrO₂ implants generated by the proper surface modification can influence early bone response and long-term sustainability.

In this study, the authors used 10-day and 28-day healing periods for bone formation in a rabbit tibia model based on previous studies^{47,48}. These healing periods of rabbit specimens are equivalent to 1-month and 3-month healing periods of humans, according to Roberts, who demonstrated that the bone healing of rabbits was approximately three times faster than that of humans⁴⁹. Although rabbits are regarded as commonly used and well-established animal models for investigating the osseointegration process, some disadvantages include site limitations and mismatched microstructures when compared to those of human bone. In addition, histomorphometric analysis has some disadvantages, although BIC and BA have become the most popular parameters. For example, they are only measured in 2 dimensions without consideration of the entire implant, and they may be affected by the quality and quantity of the surrounding bones⁵⁰. There were slight discrepancies in the geometry of the ZrO₂ and Ti implants that might have affected the tissue reaction at the bone–implant interface. The small sample size employed in this study also presents a limitation. The absence of significant differences observed in the in vivo experiments could be attributed to this small sample size. Further studies are needed to develop methods for the predictable early bone response and long-term osseointegration of IM ZrO₂ implants with a double-blinded study design and a larger sample size. Furthermore, it is needed to investigate the optimal surface roughness of ZrO₂ implants for osseointegration in subsequent studies.

Conclusion

Based on the findings of this study, it is evident that appropriate surface treatment of ZrO₂ implants is essential for promoting early peri-implant bone formation. Considering the recognized advantages of simplicity, mass production capability, and economic feasibility associated with the injection molding technique, utilizing injection molded zirconia dental implants, coupled with suitable surface modifications, could present a promising alternative to conventionally manufactured titanium dental implants for future clinical applications.

Data availability

All data generated or analyzed during this study are included in this published article.

Received: 8 March 2023; Accepted: 7 July 2023

Published online: 10 July 2023

References

- Albrektsson, T., Brånemark, P. I., Hansson, H. A. & Lindström, J. Osseointegrated titanium implants: Requirements for ensuring a long-lasting, direct bone-to-implant anchorage in man. *Acta Orthop. Scand.* **52**, 155–170 (1981).
- Trisi, P., Lazzara, R., Rao, W. & Rebaudi, A. bone–implant contact and bone quality: Evaluation of expected and actual bone contact on machined and osseotite implant surfaces. *Int. J. Periodontics Restor. Dent.* **22**, 535–545 (2002).
- Folkman, M., Becker, A., Meinster, I., Masri, M. & Ormianer, Z. Comparison of bone-to-implant contact and bone volume around implants placed with or without site preparation: A histomorphometric study in rabbits. *Sci. Rep.* **10**, 12446. <https://doi.org/10.1038/s41598-020-69455-4> (2020).
- Adell, R., Lekholm, U., Rockler, B. R. & Brånemark, P. I. A 15-year study of osseointegrated implants in the treatment of the edentulous jaw. *Int. J. Oral Surg.* **10**, 387–416 (1981).

5. Velasco-Ortega, E. *et al.* Comparison between sandblasted acid-etched and oxidized titanium dental implants: In vivo study. *Int. J. Mol. Sci.* **20**, 3267. <https://doi.org/10.3390/ijms20133267> (2019).
6. Cervino, G. *et al.* Sandblasted and acid etched titanium dental implant surfaces systematic review and confocal microscopy evaluation. *Materials* **12**, 1763. <https://doi.org/10.3390/ma12111763> (2019).
7. Albrektsson, T., Chrcanovic, B., Mölne, J. & Wennerberg, A. Foreign body reactions, marginal bone loss and allergies in relation to titanium implants. *Eur. J. Oral Implantol.* **11**(Suppl 1), S37–S46 (2018).
8. Chopra, D., Jayasree, A., Guo, T., Gulati, K. & Ivanovski, S. Advancing dental implants: Bioactive and therapeutic modifications of zirconia. *Bioact. Mater.* **13**, 161–178 (2022).
9. Comisso, I., Arias-Herrera, S. & Gupta, S. Zirconium dioxide implants as an alternative to titanium: A systematic review. *J. Clin. Exp. Dent.* **13**, e511–e519 (2021).
10. de Moura Costa, P. V. *et al.* Is zirconia better than titanium abutments for soft tissue color? A systematic review and meta-analysis of spectrophotometric evaluation. *Int. J. Oral Maxillofac. Implants* **36**, 875–884 (2021).
11. Monzavi, M. *et al.* Influence of artificial aging on mechanical properties of commercially and non-commercially available zirconia dental implants. *J. Mech. Behav. Biomed. Mater.* **101**, 103423. <https://doi.org/10.1016/j.jmbbm.2019.103423> (2020).
12. Roehling, S., Schlegel, K. A., Woelfler, H. & Gahlert, M. Zirconia compared to titanium dental implants in preclinical studies—a systematic review and meta-analysis. *Clin. Oral Implants Res.* **30**, 365–395 (2019).
13. Bethke, A. *et al.* Fracture resistance of zirconia oral implants in vitro: A systematic review and meta-analysis. *Materials* **13**, 562. <https://doi.org/10.3390/ma13030562> (2020).
14. Hanawa, T. Zirconia versus titanium in dentistry: A review. *Dent. Mater. J.* **39**, 24–36 (2020).
15. Pieralli, S., Kohal, R. J., Hernandez, E. L., Doerken, S. & Spies, B. C. Osseointegration of zirconia dental implants in animal investigations: A systematic review and meta-analysis. *Dent. Mater.* **34**, 171–182 (2018).
16. Saulacic, N., Erdösi, R., Bosshardt, D. D., Gruber, R. & Buser, D. Acid and alkaline etching of sandblasted zirconia implants: A histomorphometric study in miniature pigs. *Clin. Implant Dent. Relat. Res.* **16**, 313–322 (2014).
17. Kim, H., Lee, Y. H., Kim, N. K. & Kang, I. K. Bioactive surface of zirconia implant prepared by nano-hydroxyapatite and type I collagen. *Coatings* **12**, 1335. <https://doi.org/10.3390/coatings12091335> (2022).
18. Zhang, K. & Van Le, Q. Bioactive glass coated zirconia for dental implants: A review. *J. Compos. Compd.* **2**, 10–17 (2020).
19. Guo, L. *et al.* Cytocompatibility of titanium, zirconia and modified PEEK after surface treatment using UV light or non-thermal plasma. *Int. J. Mol. Sci.* **20**, 5596. <https://doi.org/10.3390/ijms20225596> (2019).
20. Aboushelib, M. N., Salem, N. A., Taleb, A. L. & El Moniem, N. M. Influence of surface nano-roughness on osseointegration of zirconia implants in rabbit femur heads using selective infiltration etching technique. *J. Oral Implantol.* **39**, 583–590 (2013).
21. Chen, Z. *et al.* 3D printing of ceramics: A review. *J. Eur. Ceram. Soc.* **39**, 661–687 (2019).
22. Kim, J. C. & Yeo, I. L. Bone response to conventional titanium implants and new zirconia implants produced by additive manufacturing. *Materials* **14**, 4405. <https://doi.org/10.3390/ma14164405> (2021).
23. Yoshinari, M. Future prospects of zirconia for oral implants: A review. *Dent. Mater. J.* **39**, 37–45 (2020).
24. Edirishinghe, M. J. & Evans, J. R. G. Review: Fabrication of engineering ceramics by injection molding I. Materials selection. *Int. J. High Technol. Ceram.* **2**(1), 1–31 (1986).
25. Yang, J., Wang, K., Liu, G. & Wang, D. Fracture resistance of inter-joined zirconia abutment of dental implant system with injection molding technique. *Clin. Oral Implants Res.* **24**, 1247–1250 (2013).
26. Gal, C. W., Oh, J. W., Song, G. W., Shin, D. S. & Park, S. J. Rheological and thermal debinding behaviors of silicon nitride in powder injection molding. *Ceram. Int.* **45**, 16982–16991 (2019).
27. Formas, K., Kurowska, A., Janusz, J., Szczygieł, P. & Rajzer, I. Injection molding process simulation of polycaprolactone sticks for further 3D printing of medical implants. *Materials* **15**, 7295. <https://doi.org/10.3390/ma15207295> (2022).
28. Lin, S. I. E. Near-net-shape forming of zirconia optical sleeves by ceramics injection molding. *Ceram. Int.* **27**, 205–214 (2001).
29. Arlucea, N. *et al.* Zirconia versus titanium dental implants: Primary stability in-vitro analysis. *Materials* **14**, 7886. <https://doi.org/10.3390/ma14247886> (2021).
30. Chacun, D. *et al.* Histologic and histomorphometric evaluation of new zirconia-based ceramic dental implants: A preclinical study in dogs. *Dent. Mater.* **37**, 1377–1389 (2021).
31. Roehling, S. *et al.* Ligature-induced peri-implant bone loss around loaded zirconia and titanium implants. *Int. J. Oral Maxillofac. Implants* **34**, 357–365 (2019).
32. Nishihara, H., Adanez, M. H. & Att, W. Current status of zirconia implants in dentistry: Preclinical tests. *J. Prosthodont. Res.* **63**, 1–14 (2019).
33. Choi, J. Y., Kang, S. H., Kim, H. Y. & Yeo, I. L. Control variable implants improve interpretation of surface modification and implant design effects on early bone responses: An in vivo study. *Int. J. Oral Maxillofac. Implants* **33**, 1033–1040 (2018).
34. Chevalier, J., Gremillard, L., Virkar, A. V. & Clarke, D. R. The tetragonal-monoclinic transformation in zirconia: Lessons learned and future trends. *J. Am. Ceram. Soc.* **92**, 1901–1920 (2009).
35. Gil, J. *et al.* Comparison of zirconia degradation in dental implants and femoral balls: An X-ray diffraction and nanoindentation study. *Int. J. Implant Dent.* **7**, 103. <https://doi.org/10.1186/s40729-021-00383-2> (2021).
36. Percie du Sert, N. *et al.* The ARRIVE guidelines 20: Updated guidelines for reporting animal research. *PLoS Biol.* **18**, e3000410. <https://doi.org/10.1371/journal.pbio.3000410> (2020).
37. Donath, K. & Breuner, G. A method for the study of undecalcified bones and teeth with attached soft tissues. The Säge-Schliff (sawing and grinding) technique. *J. Oral Pathol.* **11**, 318–326 (1982).
38. Gruber, H. E. Adaptations of Goldner's Masson trichrome stain for the study of undecalcified plastic embedded bone. *Biotech. Histochem.* **67**, 30–34 (1992).
39. Sim, J. H. & Yeo, I. S. Light microscopy analysis of bone response to implant surfaces. *Micros. Today.* **24**, 28–33 (2016).
40. Thomé, G. *et al.* Osseointegration of a novel injection molded 2-piece ceramic dental implant: A study in minipigs. *Clin. Oral Investig.* **25**, 603–615 (2021).
41. Janner, S. F. M. *et al.* Bone response to functionally loaded, two-piece zirconia implants: A preclinical histometric study. *Clin. Oral Implants Res.* **29**, 277–289 (2018).
42. Park, Y. S., Chung, S. H. & Shon, W. J. Peri-implant bone formation and surface characteristics of rough surface zirconia implants manufactured by powder injection molding technique in rabbit tibiae. *Clin. Oral Implants Res.* **24**, 586–591 (2013).
43. Mihatovic, I., Golubovic, V., Becker, J. & Schwarz, F. Bone tissue response to experimental zirconia implants. *Clin. Oral Investig.* **21**, 523–532 (2017).
44. Schünemann, F. H. *et al.* Zirconia surface modifications for implant dentistry. *Mater. Sci. Eng. C Mater. Biol. Appl.* **98**, 1294–1305 (2019).
45. Choi, J. Y., Albrektsson, T., Jeon, Y. J. & Yeo, I. S. Osteogenic cell behavior on titanium surfaces in hard tissue. *J. Clin. Med.* **8**, 604. <https://doi.org/10.3390/jcm8050604> (2019).
46. De Tullio, I., Berardini, M., Di Iorio, D., Perfetti, F. & Perfetti, G. Comparative evaluation among laser-treated, machined, and sandblasted/acid-etched implant surfaces: An in vivo histologic analysis on sheep. *Int. J. Implant Dent.* **6**, 7. <https://doi.org/10.1186/s40729-019-0204-4> (2020).
47. Lee, J. B. *et al.* The effect of ultraviolet photofunctionalization on a titanium dental implant with machined surface: An in vitro and in vivo study. *Materials.* **12**, 2078. <https://doi.org/10.3390/ma12132078> (2019).

48. Trindade, R. *et al.* Bone immune response to materials, part II: Copper and polyetheretherketone (PEEK) compared to titanium at 10 and 28 days in rabbit tibia. *J. Clin. Med.* **8**, 814. <https://doi.org/10.3390/jcm8060814> (2019).
49. Roberts, W. E., Smith, R. K., Zilberman, Y., Mozsary, P. G. & Smith, R. S. Osseous adaptation to continuous loading of rigid endosseous implants. *Am. J. Orthod.* **86**, 95–111 (1984).
50. Hong, J. M., Kim, U. G. & Yeo, I. L. Comparison of three-dimensional digital analyses and two-dimensional histomorphometric analyses of the bone–implant interface. *PLoS ONE* **17**, e0276269. <https://doi.org/10.1371/journal.pone.0276269> (2022).

Author contributions

I.L.Y. conceptualized this study. M.K.T., Y.S.K., J.M.K. and Y.H.J. performed the experiments. M.K.T., J.M.K. and I.L.Y. analyzed and interpreted the data. M.K.T., Y.S.K. and J.M.K. were major contributors in writing the manuscript. Y.S.K., Y.H.J., J.S.H. and I.L.Y. reviewed and edited the manuscript. M.K.T., Y.S.K. and J.M.K. contributed equally to this work. All authors read and approved the final manuscript.

Funding

This work was supported by the Korea Medical Device Development Fund grant funded by the Korean government (the Ministry of Science and ICT, the Ministry of Trade, Industry and Energy, the Ministry of Health & Welfare, and the Ministry of Food and Drug Safety) (Project number: 1711138190, KMDF_RS-2020-KD000105), and by the National Research Foundation of Korea (NRF) Grant funded by the Korean government (MSIT) (No. 2021R1A2C200465011).

Competing interests

The authors declare no competing interests.

Additional information

Supplementary Information The online version contains supplementary material available at <https://doi.org/10.1038/s41598-023-38432-y>.

Correspondence and requests for materials should be addressed to I.-S.L.Y.

Reprints and permissions information is available at www.nature.com/reprints.

Publisher's note Springer Nature remains neutral with regard to jurisdictional claims in published maps and institutional affiliations.



Open Access This article is licensed under a Creative Commons Attribution 4.0 International License, which permits use, sharing, adaptation, distribution and reproduction in any medium or format, as long as you give appropriate credit to the original author(s) and the source, provide a link to the Creative Commons licence, and indicate if changes were made. The images or other third party material in this article are included in the article's Creative Commons licence, unless indicated otherwise in a credit line to the material. If material is not included in the article's Creative Commons licence and your intended use is not permitted by statutory regulation or exceeds the permitted use, you will need to obtain permission directly from the copyright holder. To view a copy of this licence, visit <http://creativecommons.org/licenses/by/4.0/>.

© The Author(s) 2023